

# Investigation of 1.5 kW secondary side power controlled method in a inductive wireless power transfer system

Bhukya Bhavsingh<sup>1</sup>, Suresh Babu Gotluru<sup>2</sup>, Mangu Bhukya<sup>3</sup>, Ravikumar Bhukya<sup>1</sup>

<sup>1</sup>Department of Electrical Engineering, Rajiv Gandhi University of Knowledge Technologies, Basar, India

<sup>2</sup>Department of Electrical and Electronics Engineering, Chaitanya Bharathi Institute of Technologies, Hyderabad, India

<sup>3</sup>Department of Electrical Engineering, University College of Engineering, Osmania University, Hyderabad, India

## Article Info

### Article history:

Received Jun 5, 2023

Revised Nov 10, 2023

Accepted Dec 7, 2023

### Keywords:

Constant current mode

Duty cycle control method

Inductive wireless power transfer

Load-independent current

S-S compensation

## ABSTRACT

The contemporary and utilitarianism of the existing consumer world is advancing towards the better world technical benefits in the electrical world such as wired phase to wireless phase utilizing its volatile features. This paper addresses the battery performance in constant current (CC), constant voltage (CV) through inductive wireless power transfer (IWPT) systems. To analyze this workable mode, the researcher has proposed the series-series (S-S) compensation topology which is load independent current output. While charging the battery through wireless, the coil resistance is found to be affected by the battery's current and power. To figure out a practical solution, the researcher has introduced novel closed loop bi-directional switches with duty cycle control. The existing theoretical and simulated results have been analyzed with 1.5 kW, 120 mm air-gap and 85 kHz frequency. In this connection, the researcher has self-developed a prototype to better understand the theoretical perceptions of the proposed WPT system.

This is an open access article under the [CC BY-SA](https://creativecommons.org/licenses/by-sa/4.0/) license.



## Corresponding Author:

Bhukya Bhavsingh

Department of Electrical Engineering, Rajiv Gandhi University of Knowledge and Technologies Basar

Basar, Nirmal, Telangana, India

Email: bhavsingh.eee@rgukt.ac.in

## 1. INTRODUCTION

The existing internal combustion engine (ICE) releases more harmful gases and creates unnecessary problems [1]–[4], it can be avoided by the electric vehicle (EVs) as the present solution. In that connection, there will be various charging standards like hybrid electric vehicles (HEV), mild hybrid, full hybrid, supercapacitor hybrid vehicles, and so on. For this reason, the usage of electric vehicles (EVs) dramatically increased [5]–[8]. The contact charging is not safer while charging the battery and heavy gauge cables are needed. The wireless power transfer (WPT) has many applications mainly biomedical implants, consumer electronics, and even electric vehicles, this approach can be advantageous since it does not require electrical contacts to transfer power [9], [10].

Several papers have concentrated on the design based on the coil alignment, power transfer efficiency (PTE), and performance. Devano *et al.* [11] analyzed the power transfer efficiency by using hexagonal coil arrays with misalignment status. Nafaa and Yonis [12] discussed the resonance condition in impedance matching to maintain the maximum efficiency while changing the coupling coefficient. Yamaghuci *et al.* [13] experimental design is discussed while changing the auto-tuning frequency. Alghairi *et al.* and Onishi *et al.* [14], [15] focused on an asymmetric 4-coil-resonance coupling module with multiple transmitters for high stability, maximum power transfer, and efficiency. Siddique *et al.* [16] presented an automated transmitter positioning system in a capacitive power transfer system (CPT). Shukor *et al.* [17] analyzed the effect of turn ratio, air gap length, and capacitor value at both primary and

secondary to voltage ratios with finite element analysis (FEA). Ouacha *et al.* [18] introduced a special algorithm for transferring maximum power to the wireless transfer system. Bosshard *et al.* [19] comparative evaluation of the current and voltage stress in the primary and secondary side components in the series and parallel compensated inductive power transfer system. Voglitsis *et al.* [20] proposed a bidirectional power transfer in the WPT system.

In previous literature, theoretical analysis, coil design, zero power angle, comparative assessments, and experiments have focused on transferring maximum power and higher efficiency. The secondary side power control and constant voltage (CV) or constant current (CC) are not well-researched in S-S compensation. For the charging of the battery, the secondary side power control and CV or CC are required.

The design of a secondary side power control with bidirectional switches by duty cycle control and maintaining the either CV or CC is more challenging compared with the basic topologies. The basic series-series circuit is discussed in section 2. The proposed duty cycle control in the existing model pulse generation is presented in section 3. The simulated results of a proposed WPT system are presented in section 4. Battery charging performance in CC mode in section 5. Laboratory set-up discussion in section 6. Last, the conclusions are drawn in section 7.

## 2. OPERATION PRINCIPLE OF S-S RESONANT CONVERTER WITH A BATTERY LOAD

Figure 1 shows the basic wireless electric vehicle charging structure. The transmitted coil is taking the supply from the grid and it is placed on the road also the other coil is placed inside the vehicle. Here the high-frequency full bridge inverter [21] circuit is used. To improve the maximum power transferred to the coil compensation is needed for both sides such as S-S, S-P, P-P, and P-S [22]–[24]. While using the compensation both sides reactive powers observed components are neutralized and transferred only to the active power also the transmitter and receiver voltage and current are in phase as zero power angle (ZPA) [25]. From that series-series compensation is simple and less complex to design [26]–[29].

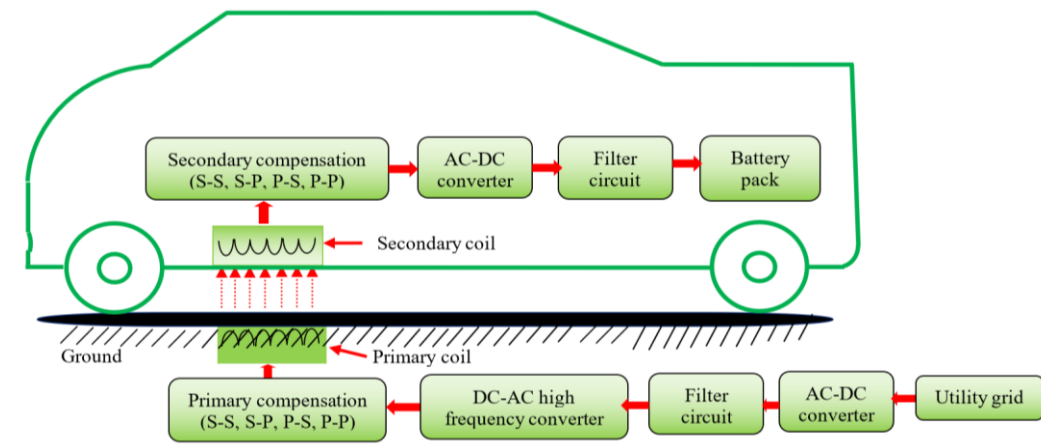


Figure 1. WPT block diagram

### 2.1. FHA analysis of S-S compensation circuit

In Figure 2(a) such as equivalent model represents the compensation capacitance  $C_1$  and  $C_2$  and Figure 2(b) such as reduced circuit represents the voltage-dependent equivalent circuit. The coil resistance  $R_1$  and  $R_2$ ,  $L_1$  and  $L_2$ , and  $M$  is mutual inductance. By applying KVL for the primary and secondary sides of Figure 2(b), the following primary and secondary currents can be written in the matrix formation in (1).

$$\begin{bmatrix} V_{AB} \\ j\omega MI_1 \end{bmatrix} = \begin{bmatrix} Z_1 & -j\omega M \\ 0 & Z_2 + R_{ac} \end{bmatrix} \begin{bmatrix} I_1 \\ I_2 \end{bmatrix} \quad (1)$$

Where,

$$Z_1 = R_1 + j\omega L_1 + \frac{1}{j\omega C_1}, Z_2 = R_2 + j\omega L_2 + \frac{1}{j\omega C_2}$$

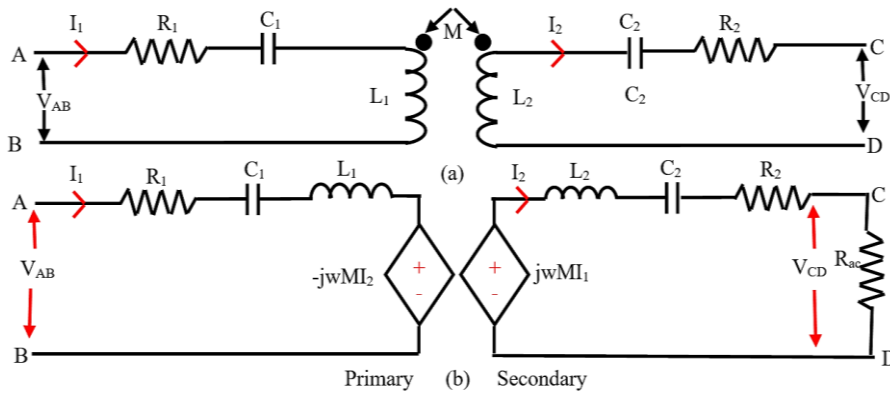


Figure 2. Basic WPT system: (a) equivalent model and (b) reduced circuit

From (1), we get the primary and secondary currents are  $I_1$  and  $I_2$  in (2).

$$I_1 = \frac{V_{AB}(Z_2 + R_{ac})}{Z_1(Z_2 + R_{ac}) + (wM)^2}, I_2 = \frac{jwMV_{AB}}{Z_1(Z_2 + R_{ac}) + (wM)^2} \quad (2)$$

In (1) and (2),  $Z_1$  and  $Z_2$  is the impedance of the primary and secondary sides, the mutual inductance representing in (3), the compensating capacitors  $C_1$  and  $C_2$  as in (4).

$$M = k\sqrt{L_1 L_2} \quad (3)$$

$$C_1 = \frac{1}{w_0^2 L_1} \text{ and } C_2 = \frac{1}{w_0^2 L_2} \quad (4)$$

At resonance, inductive reactance is equal to the capacitive reactance and neglects coil resistance in Figure 3. Apply the ohms law for Figure 3 we get the primary and secondary currents  $I_1$  and  $I_2$  in (5) and (6).

$$V_{AB} = -jw_0 M I_2$$

$$I_2 = \frac{V_{AB}}{jw_0 M} \angle 90^\circ \quad (5)$$

$$jw_0 M I_1 = R_{ac} I_2 = V_{CD}$$

$$I_1 = \frac{V_{CD}}{jw_0 M} \angle 0^\circ$$

$$I_1 = \frac{V_{AB} R_{ac}}{(w_0 M)^2} \angle 0^\circ \quad (6)$$

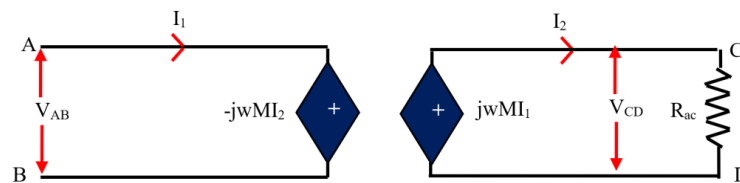


Figure 3. Resonance voltage-dependent equivalent circuit

Figure 4 shows the basic block diagram of the series-series compensation with an uncontrolled converter secondary side. The terminal shows the output of the inverter voltage  $V_{AB}$  and the rectifier input voltage  $V_{CD}$ . The (5) states that the secondary current is load independent [30]–[34]. The output power [35], can be found in (7).

$$P_{out} = P_{in} = Re(V_{AB}I_1^*) = \frac{1}{\omega_0 M} V_{AB} V_{CD} \tag{7}$$

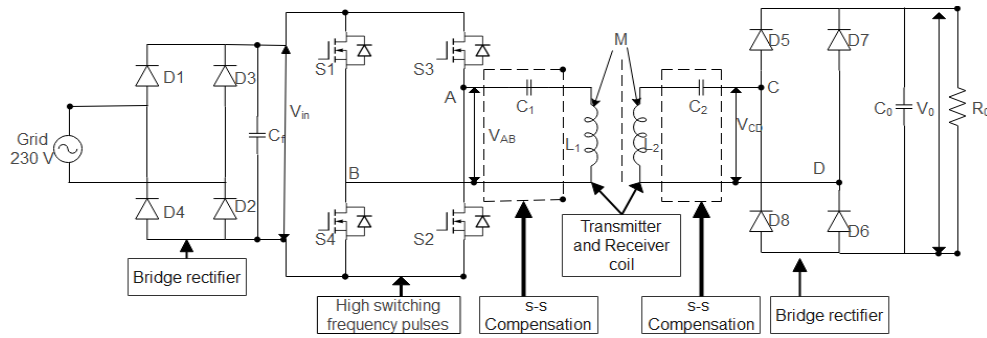


Figure 4. Basic model of S-S compensation WPT system

**3. PROPOSED TOPOLOGY AND ANALYSIS**

Figure 5 shows the bidirectional switches  $S_5$  and  $S_6$  introduced before the uncontrolled rectifier with a closed loop system to control the output power and maintain the constant current by the duty cycle controlling method. After S-S compensation the voltage is a quasi-square wave, and then the Fourier series expansion [36]–[38]. Figure 6 shows  $(\pi-\alpha)/2$  is the starting angle of the pulse,  $\alpha=D/\pi$ , D is the duty cycle. Let us take, 50% pulse width, the pulse on the period is  $90^\circ$  and the starting angle of the pulse is  $45^\circ$ . The  $V_{AB}$  and  $V_{CD}$  can be rewritten as (8) and (9).

$$V_{AB} = \sum_{k=1}^{\infty} \frac{4}{(2k+1)\pi} V_{AB} \sin((2k+1)\omega_0 t) \tag{8}$$

$$V_{CD} = \sum_{k=1}^{\infty} -\frac{4}{(2k+1)\pi} V_{CD} \sin\left(\frac{2k+1}{2}(\pi-\alpha)\right) \cos((2k+1)\omega_0 t) \tag{9}$$

Substituting (8) and (9) into (7), the output power  $P_{out}$  can be obtained as (10).

$$P_{out} = \frac{V_{AB} * V_{CD} * 8}{\pi^2 \omega_0 M} \sum_{k=0}^{\infty} \frac{\sin\left(\frac{(2k+1)}{2}\pi(1-D)\right)}{(2k+1)^3} \tag{10}$$

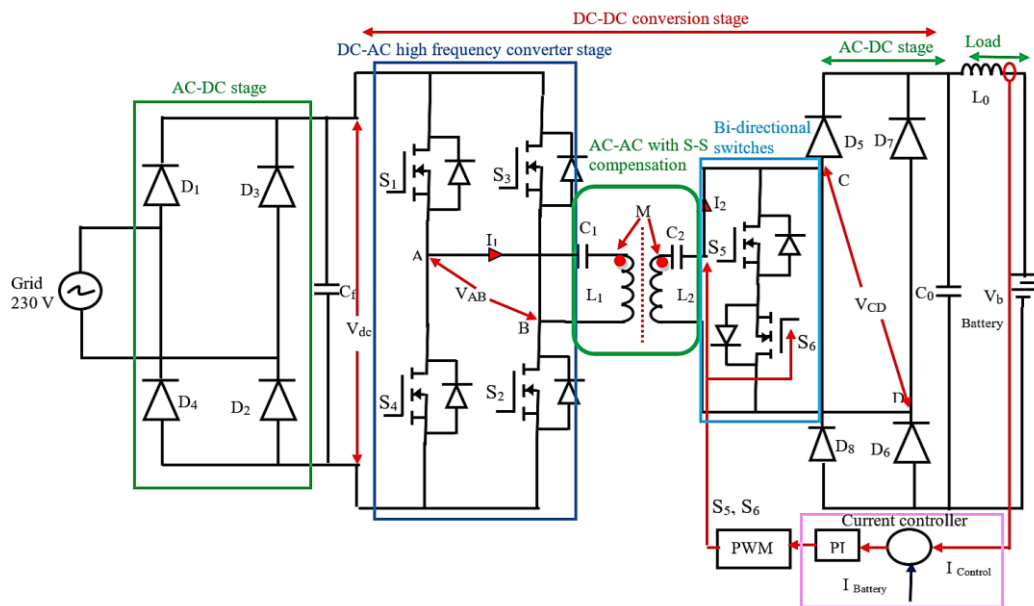


Figure 5. Secondary side power control WPT system

In (10), the output power depends on the duty cycle ( $D$ ), inverter output voltage ( $V_{AB}$ ), frequency ( $\omega_0$ ), and mutual inductance ( $M$ ) kept constant. Figure 7 shows the inverter output voltage  $V_{AB}$ ,  $S_5$ , and  $S_6$  switching pulse, rectifier input voltage ( $V_{CD}$ ), and secondary current ( $I_2$ ). These switches operate at double the resonance frequency and control the duty cycle accordingly output power was controlled but the input parameters were still constant. Total eight modes in one cycle, In the first interval  $S_5$  and  $S_6$  are in an off state, and the battery is charging through the supply, second and third intervals both switches are turned on, and the rectifier input is shorted this time battery is discharged through filter capacitor likewise total eight modes repeated the cycle.

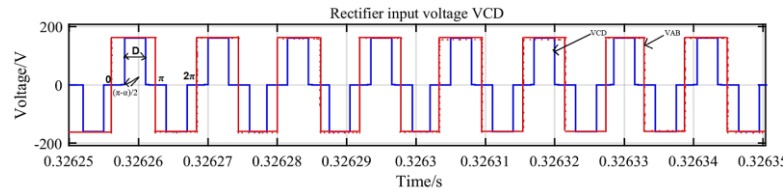


Figure 6. Rectifier input voltage and inverter output voltage

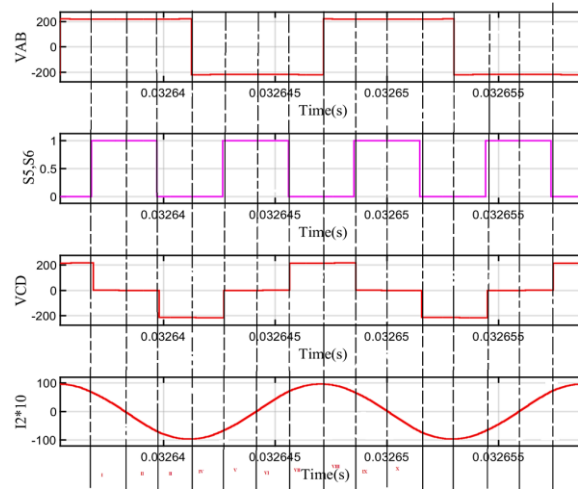


Figure 7. Bidirectional switches operating waveform

#### 4. SIMULATION RESULTS AND DISCUSSION

The values of the electrical parameters calculated in (11) to (17) are inserted in the Simulink model. The waveforms of the output voltage  $V_o$ , output current  $I_o$  and output power  $P_o$  as obtained through Simulink model are shown in Figures in sections 4.1 and 4.2, respectively.

$$L2 = Qs * \frac{R_{ac}}{\omega_0} = 6 * \frac{42.19}{2 * \pi * 85,000} = 474.22 \mu H \quad (11)$$

Where,

$$R_{ac} = \left(\frac{8}{\pi^2}\right) * \frac{V_o^2}{P_o} = 42.19 \Omega \quad (12)$$

$$L1 = \frac{M^2}{L_2 * k^2} = \frac{(62.9 * 10^{-6})^2}{474.22 * 10^{-6} * 0.16 * 0.16} = 325 \mu H \quad (13)$$

$$M = I_{srms} * \frac{R_{ac}}{I_{prms} * \omega_0} = 5.97 * \frac{42.19}{7.5 * 2 * \pi * 85000} = 62.9 \mu H \quad (14)$$

$$C_1 = \frac{1}{\omega_0^2 L_1} \Rightarrow \frac{1}{(2 \times 3.14 \times 85000)^2 \times 325 \times 10^{-6}} = 10.79 \text{ nF} \tag{15}$$

$$C_2 = \frac{1}{\omega_0^2 L_2} \Rightarrow \frac{1}{(2 \times 3.14 \times 85000)^2 \times 474.22 \times 10^{-6}} = 7.4 \text{ nF} \tag{16}$$

Quality factor and coupling coefficient can be found by (17) [39].

$$k = \left(\frac{1}{Q_s}\right) * \sqrt{1 - \left(\frac{1}{4 * Q_s^2}\right)} = \left(\frac{1}{6}\right) * \sqrt{1 - \left(\frac{1}{4 * 6^2}\right)} = 0.16 \tag{17}$$

Table 1 shows the coils structure is modeled with 3D ANSYS Maxwell software, by using those values simulating the model, for selecting the quality factor (Q) is 6 [40] is chosen for betterment of results. From Figure 8 can be observed that to avoid bifurcation-free operation is  $k < k_c$ , otherwise to get the two peaks of the frequency  $f_L$  and  $f_H$  corresponding to the output power accordingly to tune the circuit.

Table 1. FEM simulation coils quantities

Parameter	Values
Number of turns in transmitter	32
Number of turns in receiver	32
Coil diameter/mm	200mm
Self-inductance of transmitter/ $\mu$ H	325
Self-inductance of receiver/ $\mu$ H	474.22
Vertical distance varied/mm	120
Mutual inductance/ $\mu$ H	62.8
Coil	Circular
Frequency/kHz	85

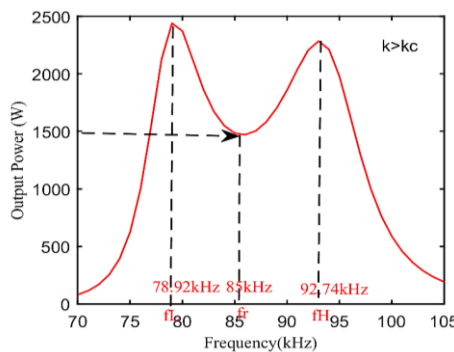


Figure 8. Output power and frequency

**4.1. Comparison of input voltage and current of the primary side and output voltage and current of the secondary side with the variation of duty cycle**

Figure 9 shows the inverter output voltage ( $V_{AB}$ ) and primary side current ( $I_1$ ), Figure 10(a) shows the rectifier input voltage ( $V_{CD}$ ) and  $I_2$  at  $D = 0$ , the switch  $S_5$  and  $S_6$  are at OFF position is the same as an uncontrolled rectifier. Figures 10(b)-10(e) is the duty cycle variation from  $D = 0$  to  $D = 1$ , the switch  $S_5$  and  $S_6$  are at ON, and the rectifier input voltage and secondary current can be controlled similarly the respective DC output voltage, current and power are changed but the primary side inverter voltage and current are not changed.

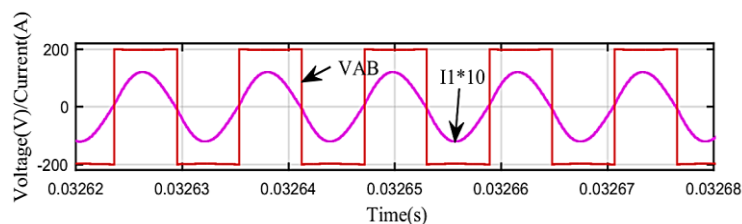


Figure 9. Inverter output voltage and current

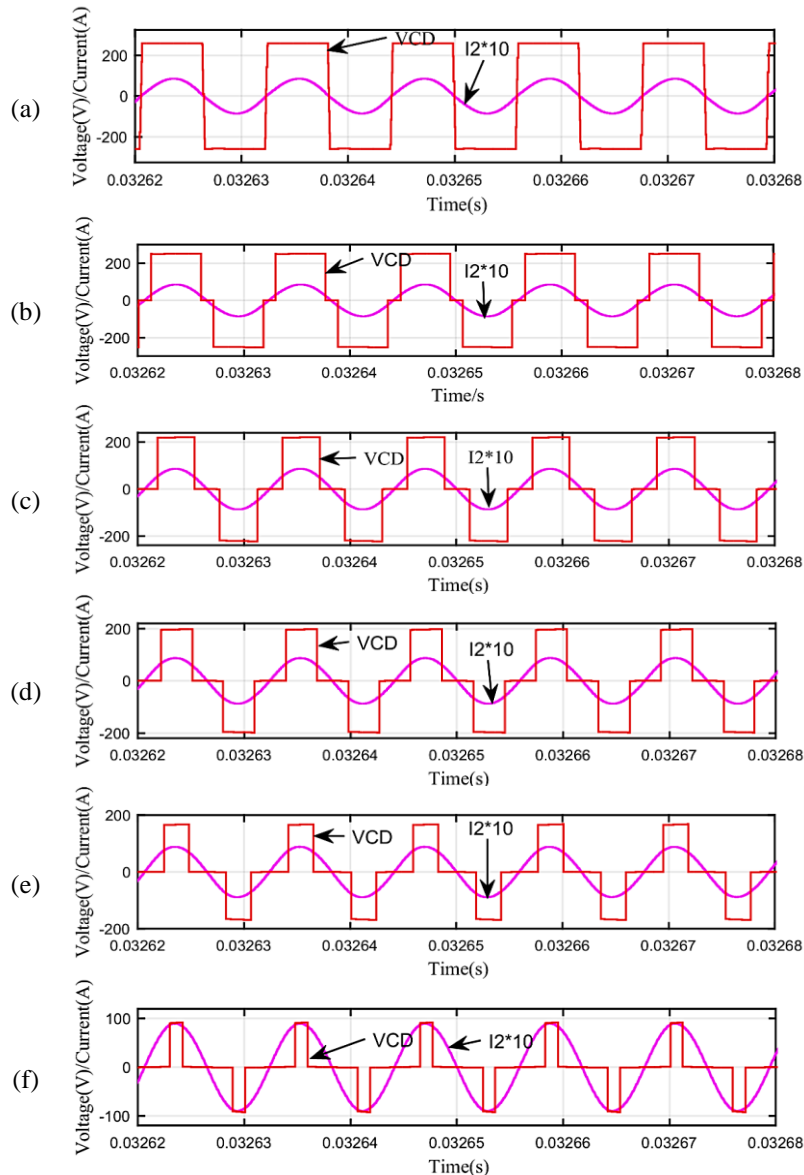


Figure 10. Rectifier input voltage and current at a duty cycle: (a)  $D = 0$ , (b)  $D = 0.2$ , (c)  $D = 0.4$ , (d)  $D = 0.5$ , (e)  $D = 0.6$ , and (f)  $D = 0.8$

#### 4.2. Comparison of the output voltage, current, power and rectifier current of the battery side with the variation of duty cycle

Figure 11 shows  $D = 0$  of the battery  $v_0$ ,  $i_0$ ,  $p_0$ , and uncontrolled bridge current, where the switches  $S_5$  and  $S_6$  are in the off position. Figure 11(a) shows the battery voltage of nearly 300 V. Figure 11(b) shows the output DC battery current is nearly 5 A. Figure 11(c) shows the DC battery output power is nearly 1.5 kW, and Figure 11(d) shows the rectifier output current is the full wave.

Figure 12 shows  $D = 0.5$  of the battery  $v_0$ ,  $i_0$ ,  $p_0$ , and uncontrolled bridge current, where the switches  $S_5$  and  $S_6$  are in the off position. Figure 12(a) shows the battery voltage of nearly 200 V. Figure 12(b) shows the output DC battery current is nearly 4 A. Figure 12(c) shows the DC battery output power is nearly half, and Figure 12(d) shows the rectifier output current is the full wave. Figure 13, shows the simulated and theoretical power and duty cycle, while changing  $D$  from 0 to 1, the power is maximum to zero. Power is maximum only for  $D$  is equal to 1, which means both the switches are at off state, for power is zero at  $D$  is equal to one, both the switches are at on, get short-circuited, battery gets charged with the help of capacitor. Table 2 shows the duty ratio changing from 0 to 1, and the mathematical and simulated values of transferred power and efficiency are tabulated. Finally, the output power of the simulation results is the same as the calculation results.

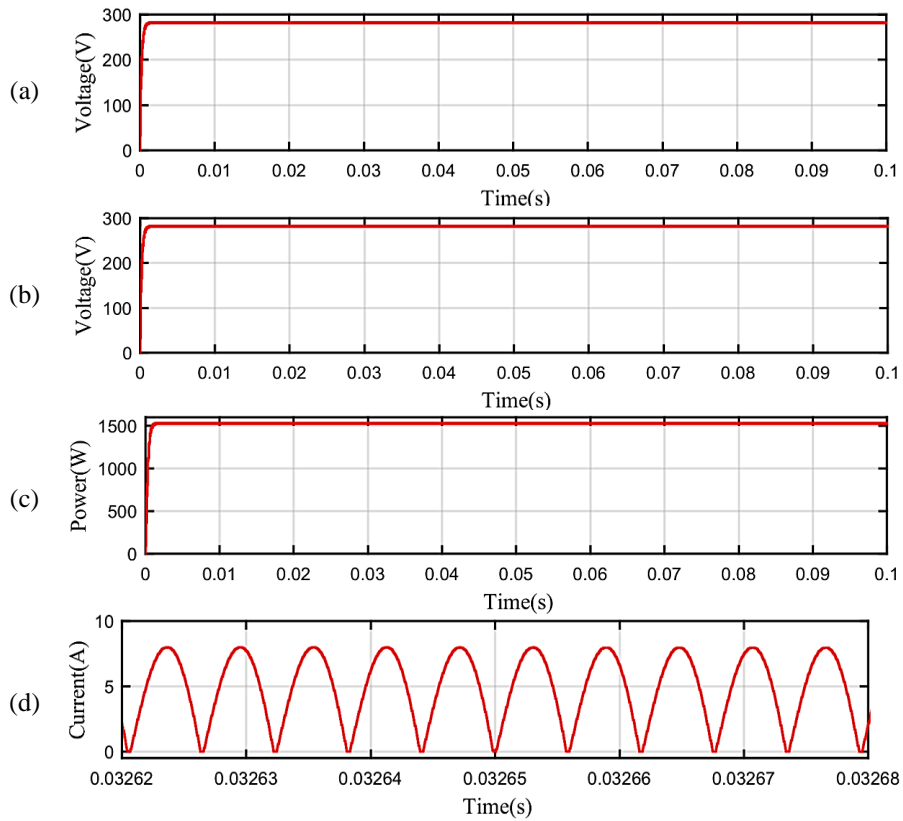


Figure 11. Output of the battery at  $D=0$  (a) output voltage ( $v_0$ ), (b) output current ( $i_0$ ), (c) output power ( $p_0$ ), (d) uncontrolled current

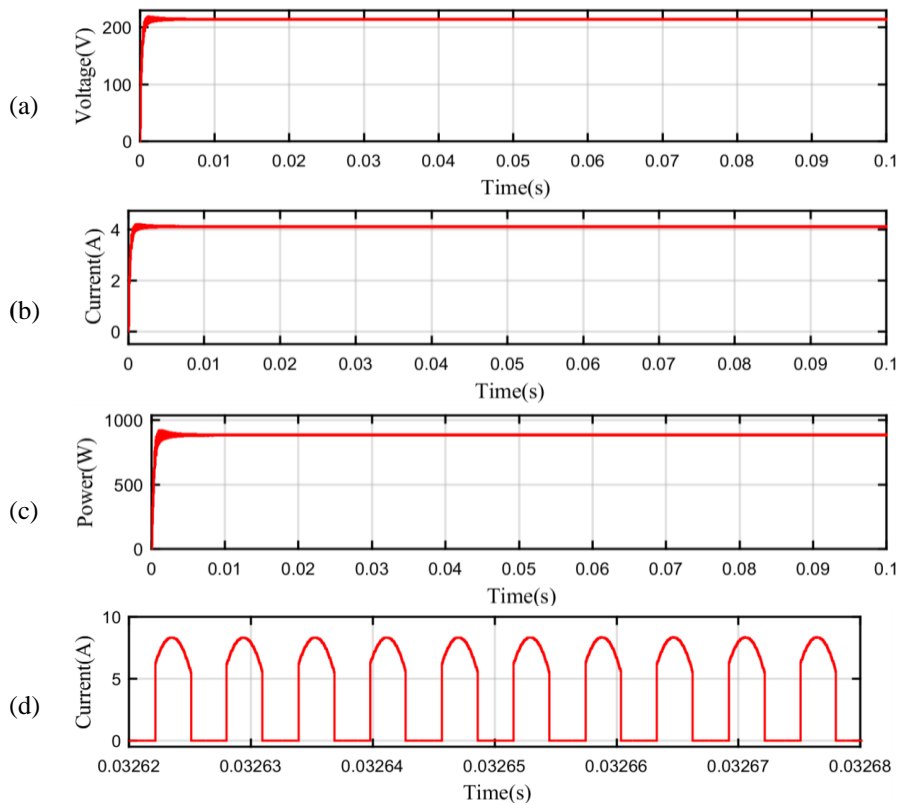


Figure 12. Output of the battery at  $D=0.5$  (a) output voltage ( $v_0$ ), (b) output current ( $i_0$ ), (c) output power ( $p_0$ ), (d) uncontrolled current



Table 2. Theoretical and simulated power and efficiency varying the D

Duty cycle D	Inverter output voltage	Rectifier input voltage	Power/W		Efficiency	Conducting angle ( $\alpha$ ) $\alpha=D*\pi$ (deg)
			Mathematical	Simulated		
0	200	268.9	1353.28	1421	96	0
0.4	200	247.9	1094.83	1075	95.44	72
0.5	200	235.7	956.91	869.3	95.26	90
0.6	200	184.5	795.44	638.7	95.02	108
0.8	200	117.9	418.188	228	92.28	144
1	200	0	0	0	0	180

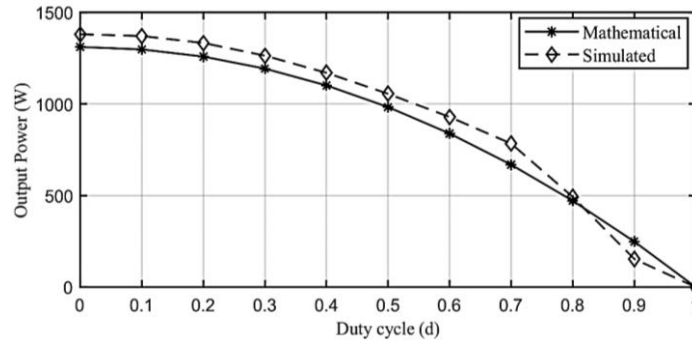


Figure 13. Output power and duty cycle

## 5. CHARGING MODES

### 5.1. Impact on the current and power while charging of battery with negligible coil resistance

Generally, in the design of the WPT systems,  $\omega_0^2 M^2 \gg R_1$ , and thus, the Secondary current is approximately constant with the variation of the load. By neglecting the  $R_1$  and  $R_2$ , (2) can be written as (18) and (19).

$$I_2 = \frac{j\omega M_0 V_{AB}}{R_1(R_2 + R_{ac}) + (\omega_0 M)^2} \quad (18)$$

$$I_2 = \frac{V_{AB}}{j\omega_0 M} \quad (19)$$

From (6) and (19): i)  $I_1$  and  $V_{AB}$  are in phase,  $I_2$  and  $V_{AB}$  have a phase difference of  $90^\circ$ ; and ii) The current of the secondary is load independent when the switching frequency is equal to the resonant frequency and the mutual inductance and the primary voltage are maintained constant but the primary current is dependent on changing of load see Figure 14 simulated and calculated primary and secondary currents. We can observe that the secondary current  $I_2$  is 5.35 A is constant for changing of battery resistance from 10 to 80, but the primary current  $I_1$  is varying. Also, the transferred power of the system is shown as (20).

$$P = \frac{(V_{AB})^2 R_L}{(\omega_0 M)^2} \quad (20)$$

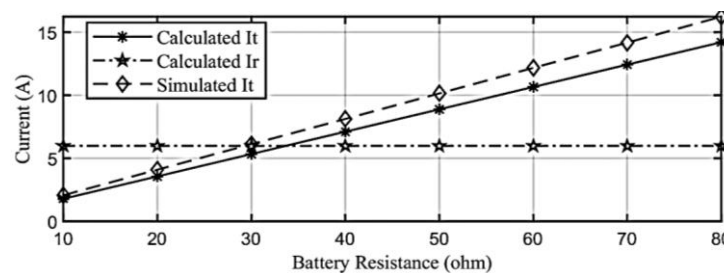


Figure 14. Primary and secondary current varying with load

**5.2. Impact on the current and power while charging of battery with changing of coil resistance**

One issue that must be considered in the design of the circuit is that the resistances of the transmitter and receiver coils affect the output current and power. In CC mode, according to (18), if the battery equivalent resistance increases, the output current  $I_2$  decreases, and the constant output operating is affected. The variation of the output current and power (20) versus the battery equivalent resistance for two different values of  $R_1$  and  $R_2$  are shown in Figures 15 and 16. It can be observed that the  $R_1$  and  $R_2$  are 1.1 ohms, the battery current is 5.439 A and 5.244 A, and the change in percentage is 3.718%, if the  $R_1$  and  $R_2$  is 1.5 ohm, the battery current is 5.329 A and 5.087 A, the change in percentage is 4.757%, also at the 50 ohm the variation for both is 5.439 to 5.329 A change in percentage is 2.06% and at 80 ohm the variation for both is 5.244 to 5.087 A change in percentage is 15.7%, this variation will be effected on the battery constant current operation also the affected on the power.

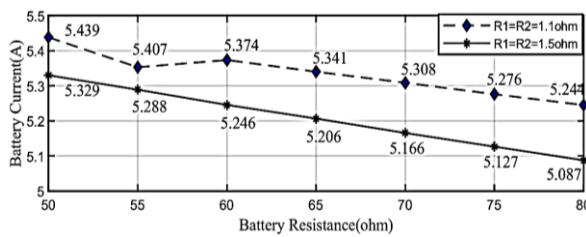


Figure 15. Variation of the battery current and battery equivalent resistance

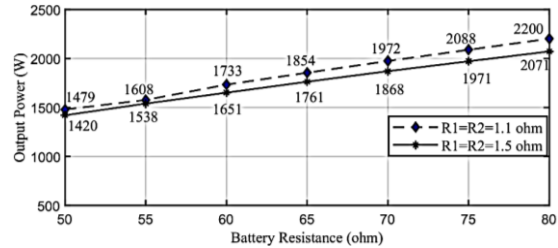


Figure 16. Variation of the output power and battery equivalent resistance

In Figure 17 when the equivalent battery resistance changes 60 % from 50 ohm to 80 ohm, the simulated battery current  $I_{bat}$  only fluctuates by 3.7% from 5.439 to 5.244 A. During the process, the simulated output power ranges from 1479 W to 2200 W. The charging profile of the battery versus battery equivalent resistance variation is shown in Figure 18. It can be observed that in the figure while charging the battery the current variation is almost constant but the voltage is increased in the WPT system.

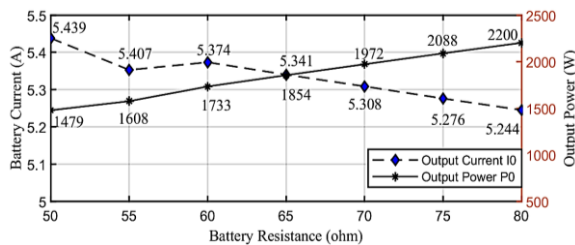


Figure 17. Battery current, output power versus batter equivalent resistance in CC working mode

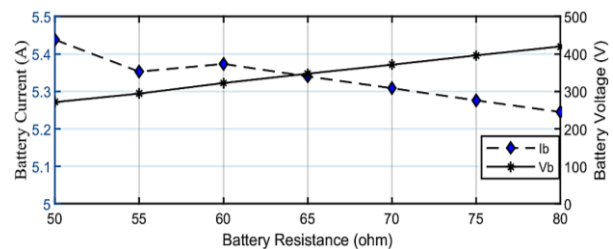


Figure 18. Battery charging profile in CC working mode

**5.3. Constant current charging mode under duty cycle control**

Figures 19, when the load resistance decreases during charging, the current parameters and transmission power are changes in (19). The secondary coil current of the S-S compensation topology remains unchanged, while the primary coil current decreases accordingly. Considering the limit situation, if a sudden fault causes a short circuit at the vehicle side (secondary side) during charging, the primary coil current will be reduced to zero.

Figure 20 shows the respective simulation results in constant current mode with step change at 1sec the load is changed from 26 ohm to 52 ohm. Figure 21 primary voltage and current as well as the load voltage and current. The output current reference of  $I_0$  is set as 4 A. When  $R_L$  is 26  $\Omega$  and the transfer efficiency of active power measured in the simulation is 87.6 %, respectively. When  $R_L$  is changed to 52  $\Omega$ , the simulated  $I_0$  is approximately 4 A. And the transfer efficiency is 91.75%, respectively.

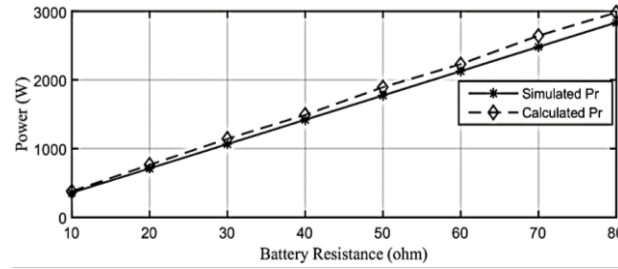


Figure 19. Transmission power varies with load

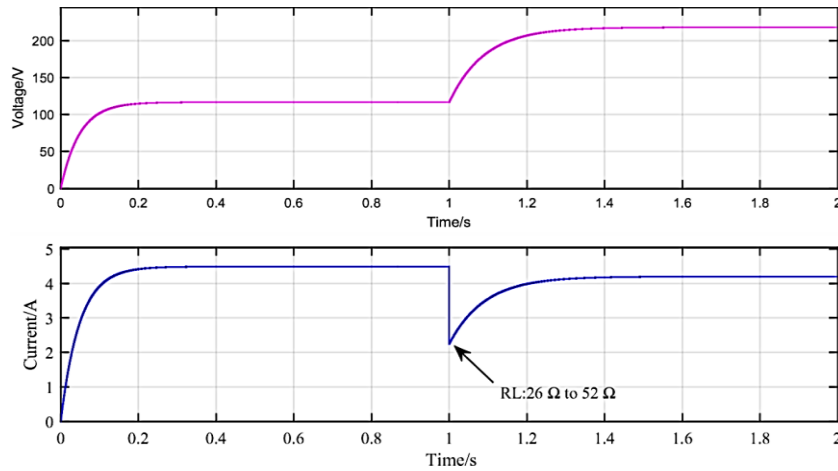


Figure 20. Simulation results of constant current charging mode under duty cycle control

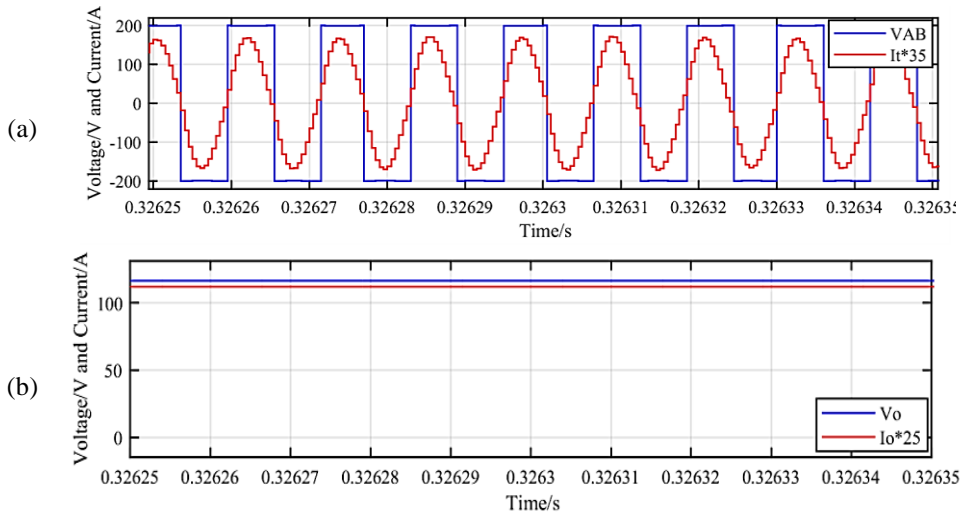


Figure 21. Operation in CC mode with S-S circuit ( $R_L = 26 \Omega$ ): (a)  $V_{AB}$  &  $I_t$  and (b)  $V_0$  &  $I_0$

Similarly, the primary current and voltage in CC mode with the battery equivalent resistance of  $26 \Omega$  are shown in Figure 21(a). Furthermore, the current and voltage of the load are illustrated in Figure 21(b). As shown in this figure, the output current is 4 A and the output voltage is around 100 V. The current and voltage waveforms of the primary in CC mode and with the output equivalent resistance of  $52 \Omega$  are presented in Figure 22(a). Also, the output voltage and current are shown in Figure 22(b). It can be seen that the output voltage is 240 V and the battery current is 4 A. During the CC mode, the current of the output is maintained constant at the level of 4 A when  $R_L$  increases from  $26 \Omega$  to  $52 \Omega$ .

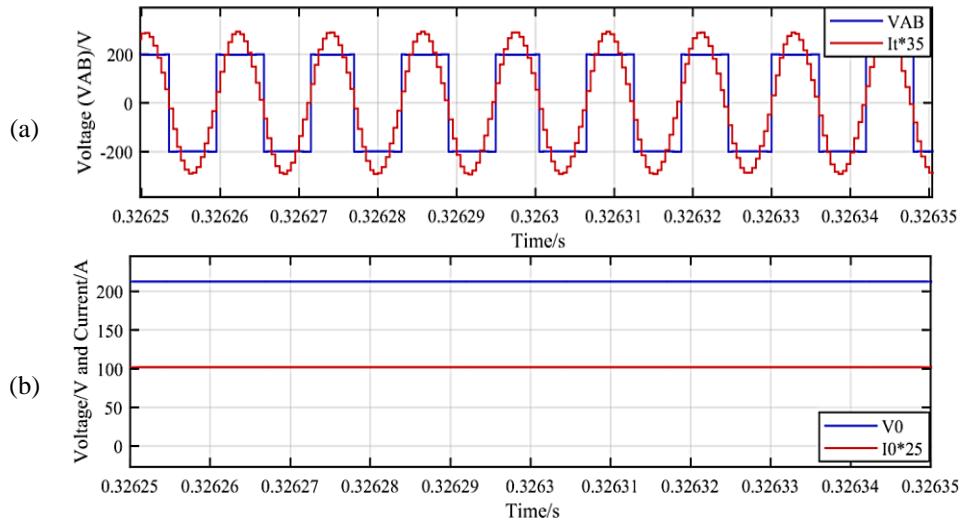


Figure 22. Operation in CC mode with S-S circuit ( $R_L=52 \Omega$ ): (a)  $V_{AB}$  &  $I_i$  and (b)  $V_0$  &  $I_0$

**6. EXPERIMENTAL RESULTS**

A small-scale prototype is designed, for the length of both coils is 400mm×400mm, and the adjustable ground clearance. The transmitter side components are a programmable microcontroller circuit, high-frequency converter, compensation, primary and secondary coil, basic full bridge rectifier, filter capacitor, and load resistance. The prototype parameters are taken from Table 1 and the experiment prototype is shown in Figure 23. Figure 24 shows the gate pulse of the MOSFET switches of the inverter. The measured inverter output voltage and transmitter current have the same phase angle shown in Figure 25.

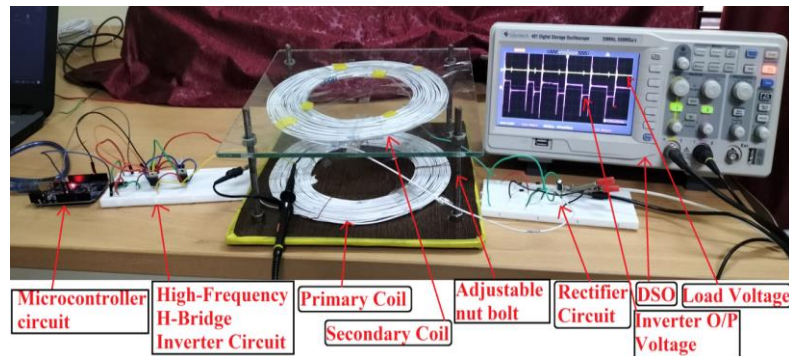


Figure 23. The small-scale prototype WPT charging system

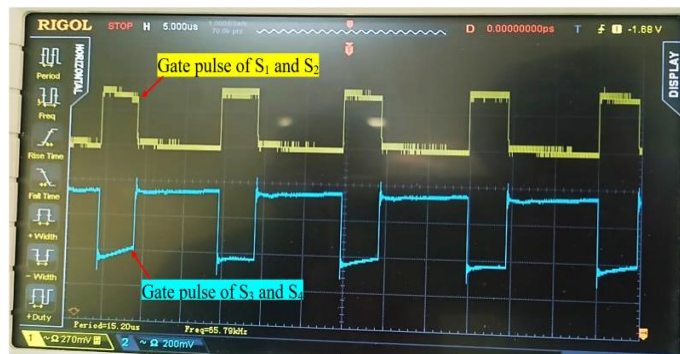


Figure 24. Measured gate pulse of MOSFETs

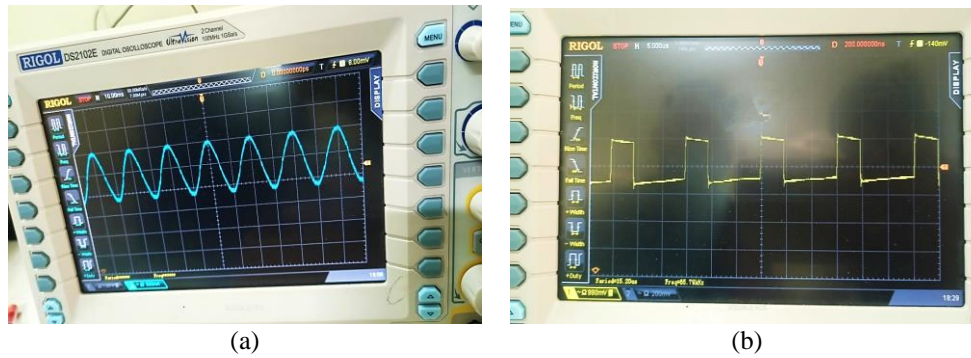


Figure 25. Measured output of inverter: (a) current and (b) voltage

## 7. CONCLUSION

In this paper, a new duty cycle control inductive wireless power transfer system has been introduced for the battery charging performance which was identified as a proposal. The S-S compensation is load-independent topology and it provides the CC charging. The important consideration is the coil resistance which affects the constant current and power of the battery. Another important consideration in designing that has been taken is the bifurcation effect which most of the IWPT charging designs have avoided. To avoid the above consideration, closed-loop duty cycle control is proposed and derived from the output power and duty cycle. Theoretical and simulated results have been observed, validated keenly, and proposed a small-scale prototype of the S-S compensation IWPT system.

## ACKNOWLEDGEMENTS

The following work was executed with the help of financial and resources available at the Department of Electrical Engineering, Rajiv Gandhi University of Knowledge and Technologies–Basar.

## REFERENCES

- [1] M. Nivas, R. K. P. Rao Naidu, D. P. Mishra, and S. R. Salkuti, "Modeling and analysis of solar-powered electric vehicles," *International Journal of Power Electronics and Drive Systems (IJPEDS)*, vol. 13, no. 1, pp. 480–487, Mar. 2022, doi: 10.11591/ijpeds.v13.i1.pp480-487.
- [2] A. Rabie, A. Ghanem, S. S. Kaddah, and M. M. El-Saadawi, "Electric vehicles based electric power grid support: a review," *International Journal of Power Electronics and Drive Systems (IJPEDS)*, vol. 14, no. 1, pp. 589–605, Mar. 2023, doi: 10.11591/ijpeds.v14.i1.pp589-605.
- [3] P. C. Balakrishna and A. S. Pillai, "Design and development of smart interoperable electric vehicle supply equipment for electric mobility," *International Journal of Electrical and Computer Engineering (IJECE)*, vol. 13, no. 3, pp. 3509–3518, Jun. 2023, doi: 10.11591/ijece.v13i3.pp3509-3518.
- [4] A. K. Karmaker, M. A. Hossain, H. R. Pota, A. Onen, and J. Jung, "Energy management system for hybrid renewable energy-based electric vehicle charging station," *IEEE Access*, vol. 11, pp. 27793–27805, 2023, doi: 10.1109/ACCESS.2023.3259232.
- [5] A. A. E. B. A. El Halim, E. H. E. Bayoumi, W. El-Khattam, and A. M. Ibrahim, "Electric vehicles: a review of their components and technologies," *International Journal of Power Electronics and Drive Systems (IJPEDS)*, vol. 13, no. 4, pp. 2041–2061, Dec. 2022, doi: 10.11591/ijpeds.v13.i4.pp2041-2061.
- [6] S. Li, P. Zhao, C. Gu, J. Li, D. Huo, and S. Cheng, "Aging mitigation for battery energy storage system in electric vehicles," *IEEE Transactions on Smart Grid*, vol. 14, no. 3, pp. 2152–2163, May 2023, doi: 10.1109/TSG.2022.3210041.
- [7] H. Polat *et al.*, "A review of DC fast chargers with BESS for electric vehicles: Topology, battery, reliability oriented control and cooling perspectives," *Batteries*, vol. 9, no. 2, p. 121, Feb. 2023, doi: 10.3390/batteries9020121.
- [8] Y. Zheng, Z. Y. Dong, Y. Xu, K. Meng, J. H. Zhao, and J. Qiu, "Electric vehicle battery charging/swap stations in distribution systems: comparison study and optimal planning," *IEEE Transactions on Power Systems*, vol. 29, no. 1, pp. 221–229, Jan. 2014, doi: 10.1109/TPWRS.2013.2278852.
- [9] Z. Zhang and H. Pang, "The era of wireless power transfer," in *Wireless Power Transfer: Principles and Applications*, Wiley, 2023, pp. 1–17. doi: 10.1002/9781119654117.ch1.
- [10] Y. Wang, Z. Sun, Y. Guan, and D. Xu, "Overview of megahertz wireless power transfer," *Proceedings of the IEEE*, vol. 111, no. 5, pp. 528–554, May 2023, doi: 10.1109/JPROC.2023.3265689.
- [11] S. T. F. Devano, T. Hidayat, and M. Alaydrus, "Improvement of power transfer efficiency of hexagonal coil arrays in misalignment conditions," *Indonesian Journal of Electrical Engineering and Computer Science*, vol. 22, no. 2, pp. 638–647, May 2021, doi: 10.11591/ijeecs.v22.i2.pp638-647.
- [12] R. E. Nafaa and A. Z. Yonis, "Magnetic resonance coupling wireless power transfer for green technologies," *Indonesian Journal of Electrical Engineering and Computer Science*, vol. 26, no. 1, pp. 289–295, Apr. 2022, doi: 10.11591/ijeecs.v26.i1.pp289-295.
- [13] K. Yamaguchi, R. Okamura, H. Terada, and K. Iida, "Experimental review of an improving system on wireless power transfer via auto tuning of frequency," *International Journal of Electrical and Computer Engineering (IJECE)*, vol. 13, no. 2, pp. 1314–1319, Apr. 2023, doi: 10.11591/ijece.v13i2.pp1314-1319.




- [14] M. Alghairi, N. Sulaiman, W. Z. W. Hasan, H. Jaafar, and S. Mutashar, "Efficient wireless power transmission to remote the sensor in restenosis coronary artery," *Indonesian Journal of Electrical Engineering and Computer Science*, vol. 25, no. 2, pp. 771–779, Feb. 2022, doi: 10.11591/ijeecs.v25.i2.pp771-779.
- [15] K. Onishi, K. Yamaguchi, and K. Iida, "Wireless power transfer using multiple-transmitters for high stability for position," *International Journal of Electrical and Computer Engineering (IJECE)*, vol. 10, no. 3, pp. 2245–2249, Jun. 2020, doi: 10.11591/ijece.v10i3.pp2245-2249.
- [16] M. N. I. Siddique, N. Ahmed, S. M. Abdullah, and M. Z. R. Khan, "An automated transmitter positioning system for misalignment compensation of capacitive-coupled electric vehicles," *International Journal of Electrical and Computer Engineering (IJECE)*, vol. 12, no. 4, pp. 3505–3516, Aug. 2022, doi: 10.11591/ijece.v12i4.pp3505-3516.
- [17] F. A. Abdul Shukor, A. M. S. Ahmed Alhattami, N. A. Mohd Nasir, and C. A. Vaithilingam, "Performance analysis of wireless power transfer using series-to-series topology," *Bulletin of Electrical Engineering and Informatics*, vol. 12, no. 4, pp. 2032–2040, Aug. 2023, doi: 10.11591/eei.v12i4.4834.
- [18] B. Ouacha, H. Bouyghf, M. Nahid, and S. Abenna, "Design and miniaturization of a microsystem to power biomedical implants using grey wolf optimizer-based cuckoo search algorithm," *International Journal of Electrical and Computer Engineering (IJECE)*, vol. 13, no. 2, pp. 1329–1337, Apr. 2023, doi: 10.11591/ijece.v13i2.pp1329-1337.
- [19] R. Bosshard, U. Badstubner, J. W. Kolar, and I. Stevanovic, "Comparative evaluation of control methods for inductive power transfer," in *2012 International Conference on Renewable Energy Research and Applications (ICRERA)*, Nov. 2012, pp. 1–6. doi: 10.1109/ICRERA.2012.6477400.
- [20] D. Voglitsis, V. Prasanth, T. Todorcevic, and P. Bauer, "Theoretical analysis and experimental investigation of high frequency bidirectional CPT system," in *2014 IEEE Transportation Electrification Conference and Expo (ITEC)*, Jun. 2014, pp. 1–8. doi: 10.1109/ITEC.2014.6861771.
- [21] R. Bhukya and P. S. Kumar, "Performance analysis of modified SVPWM strategies for three phase cascaded multi-level inverter fed induction motor drive," *International Journal of Power Electronics and Drive Systems (IJPEDS)*, vol. 8, no. 2, pp. 835–843, Jun. 2017, doi: 10.11591/ijpeds.v8.i2.pp835-843.
- [22] D. Li, X. Wu, W. Gao, D. Luo, and J. Gao, "Coupler loss analysis of magnetically coupled resonant wireless power transfer system," *CES Transactions on Electrical Machines and Systems*, vol. 7, no. 1, pp. 63–72, Mar. 2023, doi: 10.30941/CESTEMS.2023.00010.
- [23] J. Rahulkumar. *et al.*, "An empirical survey on wireless inductive power pad and resonant magnetic field coupling for in-motion EV charging system," *IEEE Access*, vol. 11, pp. 4660–4693, 2023, doi: 10.1109/ACCESS.2022.3232852.
- [24] W. Li, H. Zhao, J. Deng, S. Li, and C. C. Mi, "Comparison study on SS and double-sided LCC compensation topologies for EV/PHEV wireless chargers," *IEEE Transactions on Vehicular Technology*, vol. 65, no. 6, pp. 4429–4439, Jun. 2016, doi: 10.1109/TVT.2015.2479938.
- [25] H. Ma *et al.*, "Efficiency optimization for LCC-LC compensated inductive coupling power transfer system with load-independent zero-phase-angle and constant voltage output," *International Journal of Circuit Theory and Applications*, vol. 51, no. 8, pp. 3568–3584, Aug. 2023, doi: 10.1002/cta.3591.
- [26] A. Khaligh and S. Dusmez, "Comprehensive topological analysis of conductive and inductive charging solutions for plug-in electric vehicles," *IEEE Transactions on Vehicular Technology*, vol. 61, no. 8, pp. 3475–3489, Oct. 2012, doi: 10.1109/TVT.2012.2213104.
- [27] Z. Zhang, H. Pang, A. Georgiadis, and C. Cecati, "Wireless power transfer—An overview," *IEEE Transactions on Industrial Electronics*, vol. 66, no. 2, pp. 1044–1058, Feb. 2019, doi: 10.1109/TIE.2018.2835378.
- [28] T.-D. Nguyen, S. Li, W. Li, and C. C. Mi, "Feasibility study on bipolar pads for efficient wireless power chargers," in *2014 IEEE Applied Power Electronics Conference and Exposition - APEC 2014*, Mar. 2014, pp. 1676–1682. doi: 10.1109/APEC.2014.6803531.
- [29] X. Mou, D. T. Gladwin, R. Zhao, and H. Sun, "Survey on magnetic resonant coupling wireless power transfer technology for electric vehicle charging," *IET Power Electronics*, vol. 12, no. 12, pp. 3005–3020, Oct. 2019, doi: 10.1049/iet-pel.2019.0529.
- [30] Y. Zhang, Z. Yan, T. Kan, Y. Liu, and C. C. Mi, "Modelling and analysis of the distortion of strongly-coupled wireless power transfer systems with SS and LCC–LCC compensations," *IET Power Electronics*, vol. 12, no. 6, pp. 1321–1328, May 2019, doi: 10.1049/iet-pel.2018.5542.
- [31] D. Patil, M. K. McDonough, J. M. Miller, B. Fahimi, and P. T. Balsara, "Wireless power transfer for vehicular applications: Overview and challenges," *IEEE Transactions on Transportation Electrification*, vol. 4, no. 1, pp. 3–37, Mar. 2018, doi: 10.1109/TTE.2017.2780627.
- [32] S. Li, W. Li, J. Deng, T. D. Nguyen, and C. C. Mi, "A double-sided LCC compensation network and its tuning method for wireless power transfer," *IEEE Transactions on Vehicular Technology*, vol. 64, no. 6, pp. 2261–2273, Jun. 2015, doi: 10.1109/TVT.2014.2347006.
- [33] G. Feng, Z. Liu, X. Wei, Z. Liu, X. Zhu, and S. Shao, "Study of double-sided LCC compensation wireless power transfer based on zero voltage switching," in *2020 IEEE 3rd Student Conference on Electrical Machines and Systems (SCEMS)*, Dec. 2020, pp. 713–717. doi: 10.1109/SCEMS48876.2020.9352358.
- [34] C.-S. Wang, O. H. Stielau, and G. A. Covic, "Design considerations for a contactless electric vehicle battery charger," *IEEE Transactions on Industrial Electronics*, vol. 52, no. 5, pp. 1308–1314, Oct. 2005, doi: 10.1109/TIE.2005.855672.
- [35] W. Zhang, S.-C. Wong, C. K. Tse, and Q. Chen, "Design for efficiency optimization and voltage controllability of series-series compensated inductive power transfer systems," *IEEE Transactions on Power Electronics*, vol. 29, no. 1, pp. 191–200, Jan. 2014, doi: 10.1109/TPEL.2013.2249112.
- [36] J. Liu, Y. Zhang, Z. Wang, and M. Cheng, "Design of a high-efficiency wireless charging system for electric vehicle," in *2018 1st Workshop on Wide Bandgap Power Devices and Applications in Asia (WiPDA Asia)*, May 2018, pp. 40–44. doi: 10.1109/WiPDAAsia.2018.8734657.
- [37] B. Pang, J. Deng, P. Liu, and Z. Wang, "Secondary-side power control method for double-side LCC compensation topology in wireless EV charger application," in *IECON 2017 - 43rd Annual Conference of the IEEE Industrial Electronics Society*, Oct. 2017, pp. 7860–7865. doi: 10.1109/IECON.2017.8217377.
- [38] J. T. Boys, G. A. Covic, and A. W. Green, "Stability and control of inductively coupled power transfer systems," *IEE Proceedings - Electric Power Applications*, vol. 147, no. 1, p. 37, 2000, doi: 10.1049/ip-epa:20000017.
- [39] M. K. Thukral, "Design and Simulink implementation of electrical vehicle charging using wireless power transfer technology," in *Optical and Wireless Technologies. Lecture Notes in Electrical Engineering, vol 648*, Springer, Singapore, 2020, pp. 631–640. doi: 10.1007/978-981-15-2926-9\_69.






- [40] B. Bhavsingh, B. Mangu, and G. S. Babu, "Design and analysis of a high-efficiency dual side S-S compensation topology of inductive power transfer for EV battery charging system," in *2022 IEEE 2nd International Conference on Sustainable Energy and Future Electric Transportation (SeFeT)*, Aug. 2022, pp. 1–6. doi: 10.1109/SeFeT55524.2022.9908627.

## BIOGRAPHIES OF AUTHORS






**Bhukya Bhavsingh**    is an assistant professor in the Department of Electrical and Electronic Engineering, RGUKT-IIIT, Basara, Telangana, India. He Obtained B.Tech. in Electrical and Electronics Engineering from Vaagdevi College of Engineering, Warangal in 2009 and M.Tech. in Power Electronics in 2012 from Vaagdevi College of Engineering Warangal. He Pursuing Ph.D. in Department of Electrical Engineering, University College of Engineering, Osmania University, Hyderabad, India. His research interests include power electronics, DC-DC converters, electrical vehicles, and wireless transmission. He has more than 5 publications in international journals and has attended and presented papers in national conferences. He can be contacted at email: bhavsingh.eee@rgukt.ac.in.






**Suresh Babu Gotluru**    is a professor of Electrical Engineering at the Department of Electrical and Electronics Engineering and Chaitanya Bharathi Institute of Technology (CBIT), Hyderabad. He received Ph.D. in 2013 and a master's degree in electrical engineering from Osmania University, Hyderabad, in 2001. His research interest is electric drives, energy management, and renewable energy. He can be contacted at email: gsureshbabu\_eee@cbit.ac.in.



**Mangu Bhukya**    is a professor of Electrical Engineering at the Department of Electrical Engineering and Process, University College of Engineering, Osmania University, Hyderabad. He received Ph.D. in 2016 from IIT Bombay and a master's degree in Electrical Engineering from University College of Engineering (OU), in 2002. His research interest is renewable energy, electric vehicles, and power electronics converters. He can be contacted at email: mangu.b@uceou.edu.



**Ravikumar Bhukya**    is a Guest Faculty in the Department of Electrical and Electronic Engineering, RGUKT-IIIT, Basara, Telangana, India. He Obtained B.Tech. in Electrical and Electronics Engineering from JNTUH in 2010 and M.Tech. in Power and Industrial Drives in 2013 from JNTUH. He received Ph.D. in 2023 from Department of Electrical Engineering, University College of Engineering, Osmania University, Hyderabad, India. His research interests include power electronics, drives, power converters, multi-level inverter, EV, wireless transmission, and special machines. He has more than 10 publications in international journals and has attended and presented papers in 6 national conferences. He can be contacted at email: ravikumarb.phd@uceou.edu.